

Elementary Model of Nose Gear Retraction and Oleo-Pneumatic Strut Compression

**Brian K. Beachkofski
School of Aerospace Engineering
AE 8500
Summer 1999**

Prof. Olivier Bauchau

6 Aug 1999

DISTRIBUTION STATEMENT A
Approved for Public Release
Distribution Unlimited

20000308 013

DTIC QUALITY INSPECTED 3

REPORT DOCUMENTATION PAGE			Form Approved OMB No. 0704-0188
Public reporting burden for this collection of information is estimated to average 1 hour per response, including the time for reviewing instructions, searching existing data sources, gathering and maintaining the data needed, and completing and reviewing the collection of information. Send comments regarding this burden estimate or any other aspect of this collection of information, including suggestions for reducing this burden, to Washington Headquarters Services, Directorate for Information Operations and Reports, 1215 Jefferson Davis Highway, Suite 1204, Arlington, VA 22202-4302, and to the Office of Management and Budget, Paperwork Reduction Project (0704-0188), Washington, DC 20503.			
1. AGENCY USE ONLY (Leave blank)	2. REPORT DATE 17.Feb.00	3. REPORT TYPE AND DATES COVERED MAJOR REPORT	
4. TITLE AND SUBTITLE ELEMENTARY MODEL OF NOSE GEAR RETRACTION AND OLEO-PNEUMATIC STRUT COMPRESSION		5. FUNDING NUMBERS	
6. AUTHOR(S) 2D LT BEACHKOFSKI BRIAN K			
7. PERFORMING ORGANIZATION NAME(S) AND ADDRESS(ES) GEORGIA INSTITUTE OF TECHNOLOGY		8. PERFORMING ORGANIZATION REPORT NUMBER	
9. SPONSORING/MONITORING AGENCY NAME(S) AND ADDRESS(ES) THE DEPARTMENT OF THE AIR FORCE AFIT/CIA, BLDG 125 2950 P STREET WPAFB OH 45433		10. SPONSORING/MONITORING AGENCY REPORT NUMBER FY00-68	
11. SUPPLEMENTARY NOTES			
12a. DISTRIBUTION AVAILABILITY STATEMENT Unlimited distribution In Accordance With AFI 35-205/AFIT Sup 1		12b. DISTRIBUTION CODE	
13. ABSTRACT (Maximum 200 words)			
14. SUBJECT TERMS		15. NUMBER OF PAGES 25	16. PRICE CODE
17. SECURITY CLASSIFICATION OF REPORT	18. SECURITY CLASSIFICATION OF THIS PAGE	19. SECURITY CLASSIFICATION OF ABSTRACT	20. LIMITATION OF ABSTRACT

Abstract

Landing gear systems have two major non-linear components that need to be modeled in order to fully represent a complete landing profile, the extension actuator and the oleo-pneumatic strut. In order to test the equations of motion, the components were put together as part of a system similar to the F-15 nose gear. Working Model tested the geometry, yielding a geometry specific force-time diagram that compares well to experimental results. A real system's actuator follows a control system input, which is designed to follow a force-displacement path. The equations governing a typical actuator are integrated to compare two models: a simplified model and one that assumes no leaking nor compressibility of the fluid. The strut acts as a spring-mass system, with a non-linear spring and a damper proportional to the square of the velocity. The strut equations of motion are formulated as well as the constraints for both constant velocity and a simulated drop test. These equations are also integrated to show either a force-displacement or time-displacement diagrams. The results are then compared to the expected values for each type of test, showing data consistent with experimental and other computational methods.

Acknowledgements

I would like to thank Dr. Olivier Bauchau for his help and guidance throughout the course of this project. In addition, I would like to thank Boeing Aircraft for the help they have given both in understanding the problem conceptually and for the design drawings defining the geometry of the system in the models. Without the help of all those who listened to and/or aided me, this project could not have been done. A sincere thank you is due to them.

Table of Contents

ABSTRACT	ii
ACKNOWLEDGEMENTS	ii
TABLE OF CONTENTS	1
INTRODUCTION	2
RETRACTION MODEL	3
Working Model	3
Geometry and Mass Properties	3
Constraints	4
Actuator Model	6
Simple Model	7
More Complex Model	8
Results	10
STRUT MODEL	13
Dynamical Equations	13
Spring Force	13
Hydraulic Damping	15
Friction/Leakage Damping	17
Loading Conditions	18
Constant Velocity	18
Test Drop	20
Results	21
CONCLUSIONS	24
REFERENCES	25

Introduction

The first aspect of the model is the retraction problem. The beginning of the retraction problem is starting with a realistic geometry. The F-15 nose gear was used because it was a simple system that would allow easy modeling and analysis. The approximate geometry was finalized by using Working Model. Working Model is a two-dimensional simulation package that can create an elementary model of a mechanical system. Working Model could not provide exact constraints, so the system constraints were approximate, based on what is available within the Working Model package. A better model of the actuator could yield results that are more like an actual system. Two actuator models are explored and the shortcomings of each are shown.

The strut has three major components, each of which adds to the force profile of the strut. The first is the spring force from the compression of the inert gas chamber. This is a non-linear spring force dependent on a gas constant exponent and the displacement. The next major force component is the damping force generated by the oil moving through the main orifice. The final force is a damping force created by a combination of friction and leakage around the seals between the chambers.

Two loading conditions are investigated, each representing a normal test set. The first is an initial velocity test. This test generates both force and displacement graphs that validate the equations used. The other test condition is a simulated test drop, made more complicated than the first test by adding tires and an initial free fall. It has a given initial velocity and follows a particular force displacement curve. Drop test data for a typical oleo-pneumatic strut is known and compared to the simulation test results.

Retraction Model

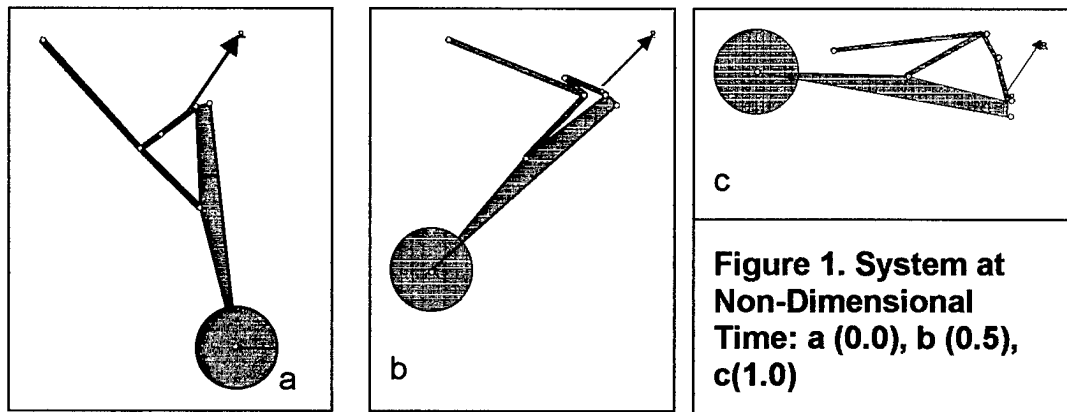
There are two main steps in the retraction model. The first is to generate a force and displacement evolution of the retraction path. A main software package used in the investigation of this problem is working model. It is a simple two-dimensional dynamic modeling tool, used to create a model of the basic system. It is not sophisticated enough to use for in-depth study of a system. It is good enough to create an initial model of the system, then was run through the retraction, and measurements taken of the actuator force. The force displacement curve is compared to experimental data.

The approximation made with Working Model as compared to the physical system is that the real actuator is neither a constant velocity, nor constant force. Simple actuator models exist and their benefits and shortcomings are pointed out through examples. The equations of motion governing the actuator are generated. These equations could be later incorporated into a complete finite element model of the whole retraction system.

Working Model

Geometry and Mass Properties

The first step in developing a model of a landing gear system is determining a realistic geometry. The geometry that will be used in this project is similar to the F-15 nose wheel gear. The data is an approximation based on design drawings, generously provided by Boeing Aircraft. The first



assumption used in generating the mass properties was that the components each have a circular cross section. Additional assumptions include each cross section is solid, except for the main strut, and a constant cross-section the entire length of the component. The configurations of the system at selected stages of retraction are shown in Figure 1.

The first assumption, that the cross-section is circular, is not far from the truth. There are only certain parts of the components that are not circular. For example, each end must have a hinge that has its axis of rotation perpendicular to the main axis of the part. The attachments to the frame have extended wings out to each side designed to create a larger moment to prevent rotation about the main axis. It is necessary for this extra mass to be close to the axis of rotation, so it does not affect the mass moment of inertia greatly.

An assumption that would greatly change things is that each cross section is solid. If the sections were not solid the amount of mass and the inertia of each piece would be significantly different from that which was used. Unfortunately, it cannot be determined if a particular piece is or is not hollow. Further, if we did assume that it is hollow, it could not be determined what the inner diameter is. So the least probable error comes from assuming a solid cross section. This is the same reason that a constant cross-section was used. It is nearly impossible to assume the correct changes in outer diameter, so the model uses a constant average cross-section diameter itself is assumed.

Constraints

The constraints are important when determining the force response of retraction. There are several forces acting on the system besides the actuator, including gravitational forces, air resistance, and hinge friction. None of these forces can be modeled exactly as they are found in an actual system, but suitable assumptions can be made to find an approximate force time plot.

The gravitational force is oriented perpendicularly down with respect to the plane's longitudinal axis. This runs roughly along the main strut when the gear is in the down position. This is

incorrect in most cases. The retraction usually occurs as soon as a positive rate of ascent is indicated. This coincides with a nose-high attitude, during which the gravitational force would be acting in a direction rotated towards the aft longitudinal axis. The load factor due to acceleration is considered to be a part of the gravitational forces because it is another body force. This magnitude and direction of the acceleration cannot be correctly assumed, but the acceleration is most likely relatively constant through the retraction. The gravitational vector and the longitudinal axis of the aircraft generate the plane that contains the acceleration vector. Because they act in the same plane, the acceleration vector acts like another variation in the direction and magnitude of the gravity vector.

The friction generated by the hinges is grouped in with the air resistance because in working model both are considered to be proportional to the rotational velocity, which is incorrect. The air resistance was increased from the normal air resistance as well because the forward velocity cannot be modeled correctly. The increase in resistance acts in the wrong direction initially when it would prevent rearward motion, because the relative wind would push the gear rearward. Even with this error, the air-resistance model increase in accuracy as the simulation continues.

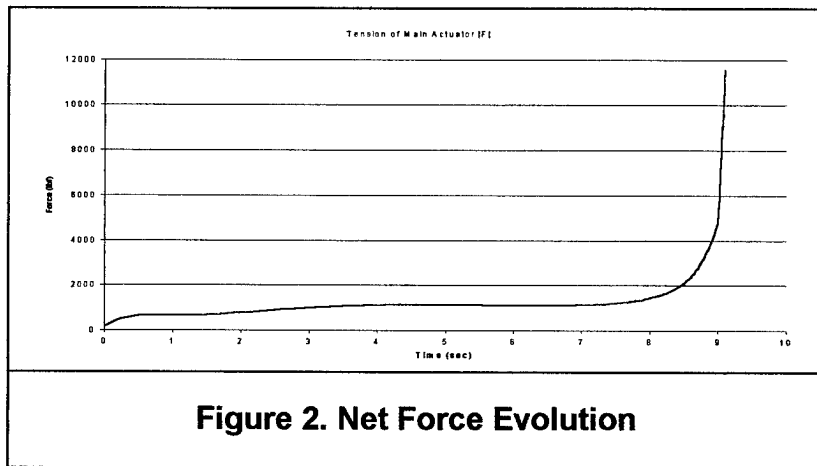


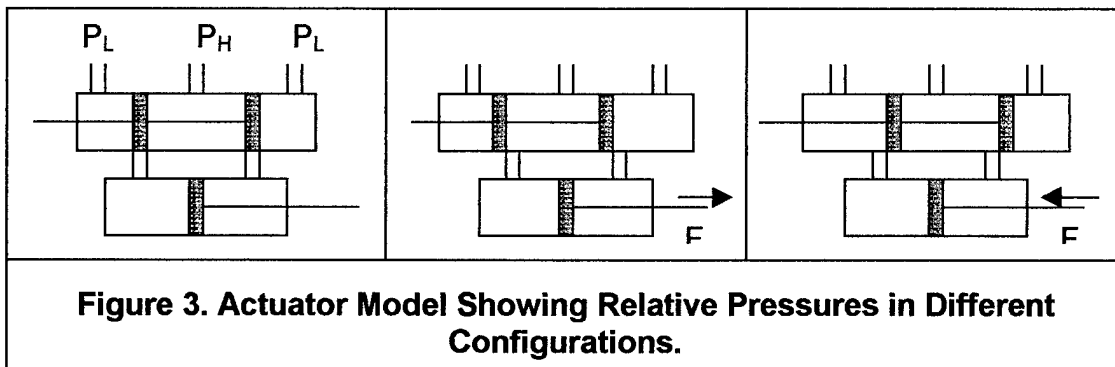
Figure 2. Net Force Evolution

Other experimental and computational data validates the assumptions, however rough they seem to be. The main difference is that the experimental data shows oscillations around the plot that Working Model produced when the locking actuator changes direction. Our model does not include a locking actuator so those oscillations will not occur. Working Model has only a constant

force or constant velocity actuator; we selected the constant velocity type. So instead of the load ending at some constant maximum load for some time, it terminates when the actuator cannot reduce in length with the constraints still satisfied.

Actuator Model

An actuator works by a high-pressure fluid being directed by a small input control, against a piston to create a large force output. An actuator does this by using a relatively small force to move a set of regulating pistons to let a high-pressure fluid into a chamber. The pressure differential across the piston causes a force output. Depending on which way the differential acts, the direction of the force will change as well. The high-pressure inlet can be directed to either side of the main piston. The below diagrams show how the system looks and would work.



A constant high-pressure inlet forces fluid into the upper chamber, and into the side opened by the movement of the input piston (upper chamber). This causes a pressure differential across the lower piston creating a net force output. The gain in output force is dependent on the pressure of the inlet and outlets, the area of the lower piston, and the efficiency coefficients for the orifices. Another important aspect demonstrated by these figures is that the sizes of the paths from the upper to the lower chambers are a function of the input piston displacement. The piston can cover a portion of the opening as it slides across it. Because of the way this works, the input signal can vary from -1 to 1 . This signal is multiplied by the cross-sectional area of the opening so that the input action can extend from completely open in one direction, to closed, to completely open in the other direction.

If the pressure differential is not large from the high-pressure side to the low-pressure side of the lower chamber, implying that the net force result is small, the fluid can be viewed as an incompressible fluid without leaking around the pistons. Further assumptions include the pressure drops across the orifices are constant and independent of the input piston displacement. This assumption is most likely a deviation from an actual system. The shape and flow around the orifice is very dependent on the amount of the orifice that is covered by the piston, and would therefore make the orifice coefficient a function of the displacement as well, but this model does not include these effects. The final assumption is that the orifice area is linear with respect to the displacement of the piston. Some physical actuators would have orifices without rectangular cross-sections, and not fall under this assumption.

Simple Model

The equations that define this system are based on the equation of flow rate through an orifice. That equation is below twice, the second time with the sundry terms combined to give a simple linear equation.

$$q = c_{ori} A_{ori} \sqrt{2g \frac{\Delta p}{\omega}} = c_x x$$

q – Flow rate through orifice
 c_{ori} – Orifice efficiency coefficient
 A_{ori} – Orifice area (width times x)
 g – Acceleration of gravity
 Δp – Pressure drop across orifice
 ω – Specific gravity of fluid
 x – Input displacement
 c_x – Inflow coefficient

Under the assumptions of incompressible flow without leakage, the flow rate into the lower chamber must equal the rate of change in volume for the chamber. As could be seen in the figures of the actuator, the output displacement is proportional to the lower chamber volume. The rates of change must also be proportional as well.

$$\dot{V} = c_y \dot{y} = q = c_x x$$

$$\dot{y} = \frac{c_x}{c_y} x$$

\dot{V} – Cylinder volume time rate of change
 c_y – Lower chamber piston area
 \dot{y} – Output velocity

The system is completely defined without mention of the mass, spring, or damping terms. This points out the assumption of small pressure differential across the lower piston. Since the input signal is the proportional to the time derivative of the output displacement, it very easy to control the output displacement. That is the main advantage of this model, but the strict limits the assumptions impose make it a poor model for most applications. The effects of these assumptions are easily seen in the results section. If the pressure drop were higher, the resisting load would be higher and could not be considered small in comparison to the forcing function.

More Complex Model

In those cases where the load is large, the assumptions of an incompressible fluid and negligible leakage become inaccurate. Under large compressive forces the fluid will compress and allow more flow without an increase in volume. In those conditions the pressure drop across the piston become significant and leaking will occur around the piston. The flow continuity equation has three parts under these conditions: incompressible, compressible, and leak flow.

The incompressible flow remains the same from the last analysis. The derivative of the output displacement is proportional to the input displacement. This analysis was covered in the previous section; the only change being that the relative pressure of the high-pressure reservoir and the output load come into effect. We assume that the reservoir is sufficiently large so that the high-pressure stays constant throughout the period of interest.

The compressible flow is equations come from the definition of the bulk modulus. The change with respect to time is explored at the limit when it approaches zero to produce the differential equation used in the model. The time change in volume is not an actual change in volume, but a reduction in the fluid volume, which will be equal to the inflow rate.

$$K_B = \frac{\Delta P_L}{\Delta V/V}$$

$$\frac{\Delta V}{\Delta t} = \frac{V}{K_B} \frac{\Delta P_L}{\Delta t}$$

$$\dot{V} = \frac{V}{K_B} \dot{P}_L = q_{comp}$$

K_B – Fluid bulk modulus
 P_L – Pressure in lower chamber
 V – Volume in lower chamber
 q_{comp} – Effective flow rate from fluid compression
 t – Time

The leakage terms build themselves from the assumptions in the previous case. When the pressure drop across the piston is small, the amount of fluid leaking will be small. The amount that leaks increases with the pressure differential across the border. A simple estimation for this is that the leak rate is proportional to the pressure differential.

$$q_{leak} = LP_L$$

L – Constant of proportionality
ow rate from leaking

When put together the complete equation becomes:

$$q = q_{leak} + q_{comp} + q_{incomp}$$

$$q = LP_L + \frac{V}{K_B} \dot{P}_L + C_y \dot{y}$$

$C_y - c_x/c_y$ from the incompressible flow equation.

Since the high-pressure is considered a constant, the function for flow becomes a function of two variable, x and P_L . It is shown in [7] that, when initial conditions are taken as the zero point for P_L , q, and x, the general form of the flow equation is:

$$q = c_x x - c_p P_L$$

c_x – Initial rate of change of flow with change of input signal
 c_p – Initial rate of change of flow with change of chamber pressure

The minus sign is to keep the value of both c_x and c_p positive. This equation, when paired with the equation of equilibrium for the system pictured below, define the system.

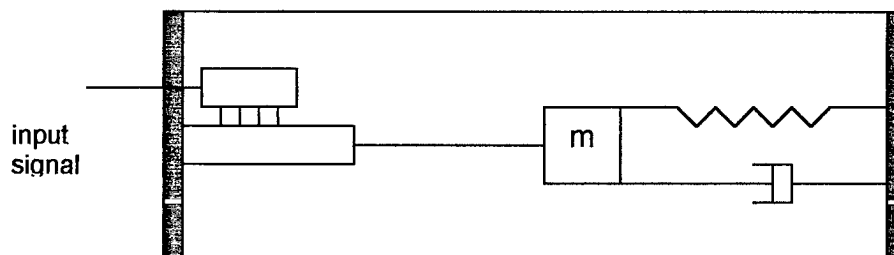


Figure 4. Actuator Model System.

The final equations of motions are:

$$\ddot{y} = \frac{C}{M} \dot{P}_L - \frac{B}{M} \dot{y} - \frac{K}{M} y$$

$$\dot{P}_L = \frac{K_B}{V} [c_x x - (L + c_p) P_L - c_b \dot{y}]$$

Results

The dynamical equations are integrated using a Runge-Kutta technique that has a time step of $2.7E-2$. The actuator system was initially at rest with an actuator length of 25 inches. The input signal is a half sine wave extended over a period of 2π . The total runtime of the simulation is 8π .

The simplified model shows that the displacement slope is clearly related only to the input signal. There is no sign of oscillations from inertial forces because they are assumed to be small in comparison with the output force, by means of the small pressure drop across the lower piston. Another key point is the fact that the actuator can hold the final position deflection. That is because the spring force holding the displacement is considered negligible so that the pressure difference across the piston is nearly zero, implying no leaking.

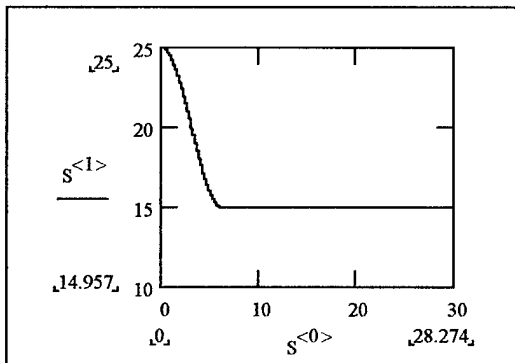


Figure 5. Output Displacement, Simplified Model.

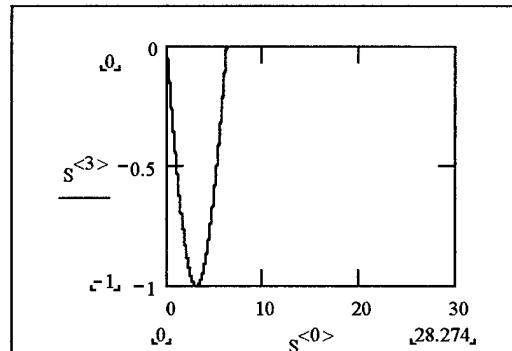


Figure 6. Input Signal, Simplified Model.

The release of the assumption that the forces acting on the displacement are negligible leads to a more complicated model that more fully represents an actual system. The oscillations from the inertia forces become important as well as the leaking around the piston. The leaking leads to the displacement returning to the initial position, while the damping forces slowly dissipate the inertia forces.

The initial oscillation looks similar to the simple model, but the subsequent time passing shows a completely different evolution. The values of the constants were chosen in such a way as to accentuate the differences between the two models, but they would exist in any system to some

degree. The inertia from the mass makes the actuator overshoot the point where the simple model stopped, and the point about which the oscillations occur slowly returned towards the initial length of the actuator.

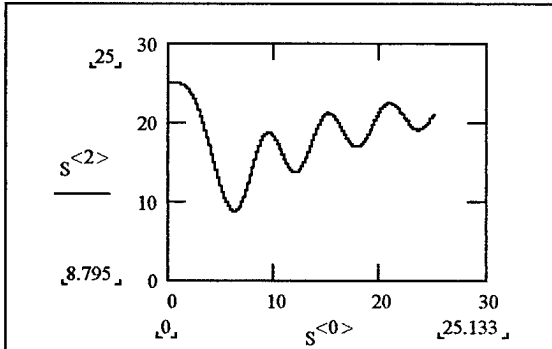


Figure 7. Output Displacement, Standard Model.

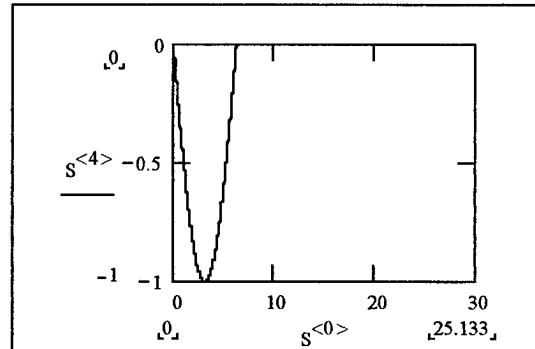


Figure 8. Input Signal, Standard Model.

In addition to the displacement and input signal, another interesting plot is the pressure differential in the chamber over time. The pressure is related to the acceleration of the displacement. If we can see that the displacement is similar to the integral of the input signal, in this case the displacement will be a cosine wave. The acceleration should therefore be similar to the second derivative of the displacement. In this example that would make the pressure a cosine wave. For the figure below you can see that the pressure does follow this predicted path as long as the input signal is non-zero.

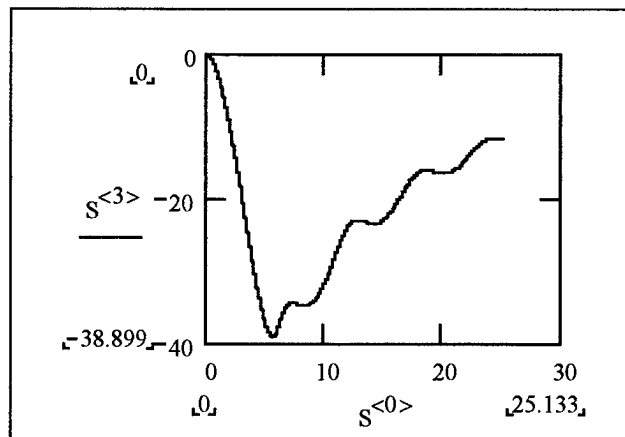


Figure 9. Chamber Pressure Evolution.

The pressure returns to neutral with the compressive oscillations about the equilibrium position. There was no purpose to have this plot in the simplistic model because the pressure difference across the piston was considered small.

There is still a great deal of improvement to be made in this model. The assumption that there is a constant pressure drop is not extent in the real system, but only made to simplify the equations. There is a way to include the variation of the flow rate depending on the pressure drop across the orifice. Another aspect of the system that is not included in the model is the friction damping. These changes were made in [5] as well as a more complex model of the compressibility effects. This new actuator model dramatically increases the complexity. The pressures in each half of the chamber are modeled separately as is each flow rate for the separate orifices.

The simplest model that can accurately reflect each wanted result should be used. Our geometry model has already made simplifications that would completely change the small dynamic forces. The need for the most complex model described in [5] is not necessary for this model.

The system should be modeled in the future, combining the actuator model described in this paper with a complete landing gear system. It would be interesting to see if the results would be substantially different with the actuator force determined by an input signal instead of the constant displacement constraint.

Strut Model

The main aspect of the landing sequence are the forces created by the compression of the main strut. This report will look at the compression of an oleo-pneumatic strut. The three main components of an oleo-pneumatic strut are the air compression spring force, the hydraulic damping force, and friction and leaking forces. Each of these parts contributes to the entire strut force. The force equations come directly from the geometry of the strut, but can be very sensitive to the estimated dimensions.

The next step is to use these equations under certain conditions that will adequately model the actual system in a given test situation. The two types of conditions that will be employed are the constant velocity model and a variation, and the drop test model. The constant velocity model is relatively trivial, because it makes the hydraulic damping and the friction forces constants. The only variable force is the spring force. The drop test is more complicated with each force being variable throughout the travel of the strut.

Several different lengths must be defined for the system. The length of the strut is measured from the mounting above the cylinder to the axle. The stroke is defined as the change in length of the strut with a positive orientation in compression. The length is called δ and the velocity of compression is the time rate of change of the length.

Dynamical Equations

The forces developed through strut compression are dependent on the geometry of the strut. Because these are mostly assumed values, they are subject to variation from the actual system.

Spring Force

The only known values from the system concerning the spring force is the length of the strut at the extended, static, and compressed lengths. From this it is possible to determine the total

stroke length. An assumed static pressure, pre-load at extension, and compressed compression ration, fully determines the air compression spring force.

From [6], the static pressure is chosen to be 1500 psi. This is a value used in industry quite commonly because it allows for the easy pressurization of the strut without much trouble. It also ensures that there will be enough spring force to overcome any static friction at the fully extended position. The compression ratios selected at full extension and full compression are rather arbitrary, and most likely far from the actual values. The values used here are in the neighborhood typically found in other aircraft of similar size, yet because the entire spring force is based on these approximations, the risk of future error is significant, but unavoidable in this situation.

The gas law is used to determine the volumes for each respective position. For these initial calculations the exponent for the gas law is one because the static loads used for these calculations are dominated by isotropic conditions. The gas law becomes:

$$P_1V_1 = P_2V_2$$

Subscripts indicate the physical configuration of an isotropic system at two different times.

Under shock loading conditions, the strut will not act like an isotropic chamber, nor will it act completely isothermal. Many studies have been performed to determine the correct exponent for the polytropic loading conditions experienced in landing. The mixing of the oil and the air produces differing exponents, but many agree on the value of 1.1 for it, including [2]. The spring force is below, with the piston area determined by dividing the static load by the static pressure.

$$F_{spring} = P_{extended} A_{piston} \left(\frac{V_{extended}}{V_{extended} - A_{piston} \delta} \right)^n$$

F_{spring} – Pneumatic spring force
 $P_{extended}$ – Pressure in air chamber when fully extended
 A_{piston} – Piston area
 $V_{extended}$ – Air chamber volume when fully extended
 δ - Strut stroke from fully extended

The force displacement graph is shown in Figure 10. A few important items should be noticed from this plot. First, the pre-load is evident and is 5000 lb. The pre-load must exist because of the finite volume limits, and is determined by requirements for strut stiffness in taxiing and any limits in the variation of weight. For example, a cargo aircraft has a large variation in weight during loading, so to prevent the strut from being fully extended whenever it is lightly loaded, the pre-load is proportionally smaller than other aircraft.

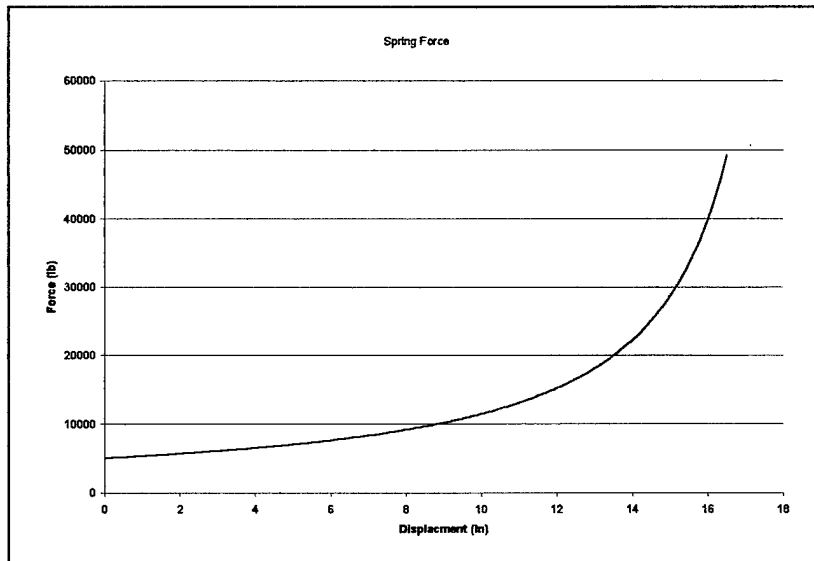


Figure 10. Spring Force-Deflection Plot

The other end of the chart is also interesting. There is no maximum load to encounter. The load increases asymptotically as the total volume goes to zero. The final note is that the spring load is increased from the static or a purely isotropic condition. For example, a ten thousand-pound static load would be produce to the 10.4-inch stroke, yet the same load corresponds to an 8.9-inch stroke under polytropic conditions as seen in Figure 10. The strut is stiffer under a dynamic load, even without the hydraulic damping effects, by acting polytropically.

Hydraulic Damping

The significant damping in the strut comes from the movement of hydraulic fluid moving from one chamber to another through a small orifice. Many times the area of this hole is controlled through

the stroke by a metering pin. A metering pin is a variable diameter pin that restricts the flow through the orifice as compression proceeds. Our simplified model does not include this factor. Many studies have shown that the use of a metering pin can drastically affect efficiency of the strut up to a maximum of around 90%.

Other factors that affect the damping coefficient are also included in the interior of the strut. Among these factors are the piston area, hydraulic fluid specific density, the orifice discharge coefficient, and the orifice area. All of these parameters can be approximated, but many depend on other approximate factors. The chance for error propagation is substantial. There is an equation that gives a good initial value for the orifice area provided by [6].

$$A_{orifice} = \frac{0.30 A_{piston}}{\frac{Appl. Load}{Stat. Load}} \sqrt{\frac{A_{piston} Stroke_{total}}{Stat. Load}}$$

A_{piston} – Piston area
 $Stroke_{total}$ – design stroke length
 $Stat. Load$ – Static load
 $Appl. Load$ – Applied load, without a metering pin maximum load

This equation is a gross approximation, as can be seen by the inconsistent units. Though it was used to determine the orifice size for this model, it can be significantly off from the real system. The applied load would normally be a function of stroke, but without the metering pin in the model the maximum expected g-load was used instead.

Several factors contribute to the damping coefficient. Again, these had to be approximated, such as the specific density of the fluid being twice that of water. This is between that of water and glycerin. The other main assumption is that the orifice discharge coefficient is 0.65. This is typical of orifices with one side of the gap filleted and the other left square. The equation governing the damping coefficient is:

$$\mu_{hyd} = \frac{\rho A_{piston}^3}{2(C_d A_{orifice})^2}$$

μ_{hyd} – Hydraulic damping coefficient
 ρ – Fluid density
 C_d – Orifice discharge coefficient

It can be shown, and it is reported in [1], that the damping is proportional to the velocity squared.

This gives the final form of the damping force to be:

$$F_{hyd} = \mu_{hyd} \dot{\delta}^2$$

$\dot{\delta}$ – Rate of stroke compression

Friction/Leakage Damping

These forces are to correct for the assumptions of a perfect, frictionless seal on the piston. This obviously does not exist in reality. It would make sense that the leakage would be proportional to the pressure differential across the seal. In [1] the authors make the approximation that this pressure difference is equal to the pressure in the air chamber. They provide an Air Force Technical Document as the source for this and leave that as the only justification for the assumption. Additionally, the seal friction force counter-acts the motion of the seal. This is a more classic assumption that is seen in many other references including [5] that deal with two chamber systems. The only parameter to be assumed is that of the friction coefficient. A ten-percent loss is typical, and the value used in this model.

$$F_{fric} = \frac{\dot{\delta}}{|\dot{\delta}|} \mu_{fric} F_{air}$$

F_{fric} – Friction force
 F_{air} – Air spring force
 μ_{fric} – Friction coefficient

This friction model is accurate in dynamic loading circumstances. Unfortunately, this model loses accuracy as the loading approaches a quasi-static loading. Under testing, this error becomes apparent when the equilibrium position is found to be quite different than the designed deflection. This is because the friction acts proportional to the spring force even in static loading. A better model would have a different function that would model friction proportional to the velocity when the velocity dropped below some arbitrary value. The function that satisfies that requirement is:

$$F_{fric} = \dot{\delta} \mu_{fric} F_{air}$$

If the friction model is chosen to be in the form shown above, the final form of the equilibrium equation is:

$$F = \frac{\dot{\delta}}{|\dot{\delta}|} \mu_{hyd} \dot{\delta}^2 + \dot{\delta} \mu_{fric} A_{piston} P_{ext} \left(\frac{V_{ext}}{V_{ext} - A_{piston} \delta} \right)^n + A_{piston} P_{ext} \left(\frac{V_{ext}}{V_{ext} - A_{piston} \delta} \right)^n$$

Loading Conditions

Constant Velocity

The constant velocity conditions create an almost trivial system to evaluate in a mathematical model, as opposed to the system that exists in an experiment. The model can give the system an initial velocity that does not exist in the real system. When the model is at a constant velocity the only non-constant part of the force is of the form of the pneumatic spring.

The real system also has mass, which would create small variations in the force needed to maintain the constant velocity. This model does not have to accelerate, nor does it carry any momentum. Most of those factors would result from the initial impact loading. The force-displacement diagram for the constant velocity case is shown in Figure 11.

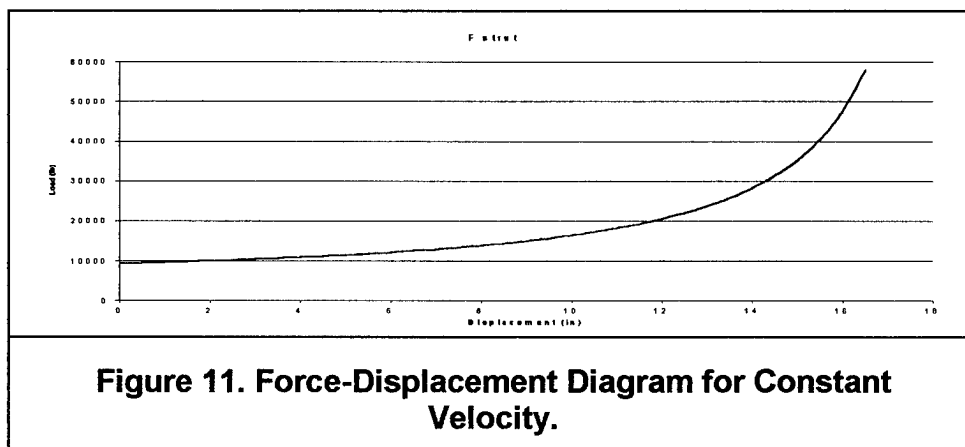


Figure 11. Force-Displacement Diagram for Constant Velocity.

In an attempt to investigate a model that would explore the effects of the impact load alone, we gave the system an initial velocity with a lumped mass attached to the end of the strut. Another Purpose for this example was to test the dually defined friction test. It is also a step closer to the drop test by attaching a lump mass on the free end of the strut and including a gravity load.

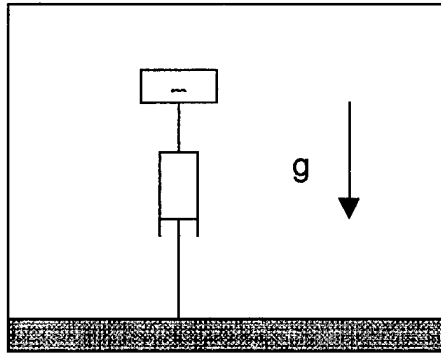


Figure 12. Test Two Configuration.

Because the velocity is not constant, the force is much greater initially, when the hydraulic damping is dominant. Otherwise, the force is relatively constant until the pneumatic force increases. This is where the main difference can be seen between the single and dual friction force. The dual friction lets the strut oscillate about the equilibrium point, instead of being overwhelmed by a ten-percent force resisting motion. That resisting force causes an unstable behavior that is seen in the force diagram. The following figures show relevant plots concerning these tests.

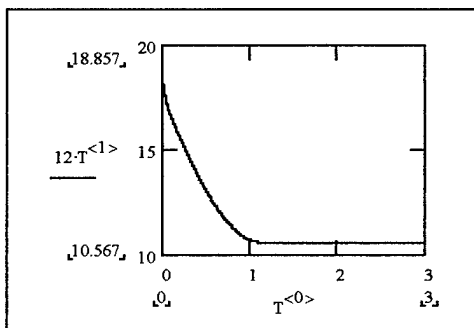


Figure 13. Displacement, Single Friction.

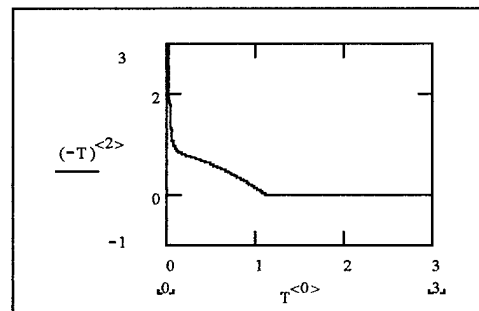


Figure 14. Velocity, Single Friction.

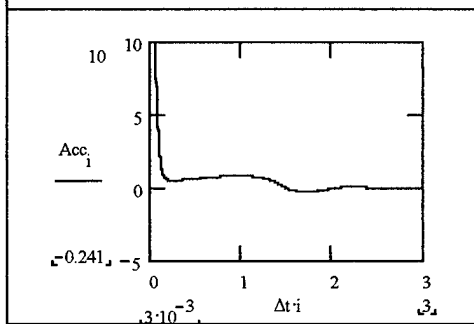


Figure 15. Acceleration, Double Friction.

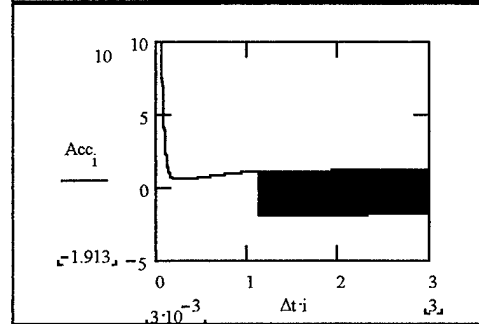


Figure 16. Acceleration, Single Friction.

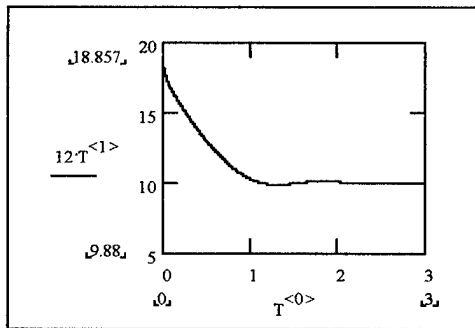


Figure 17. Displacement, Double Friction.

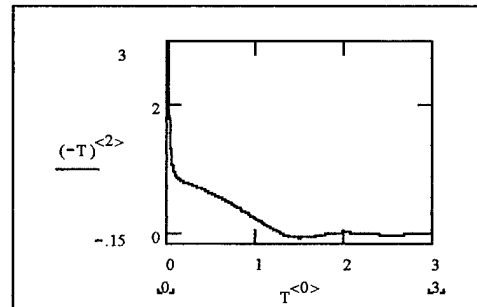


Figure 18. Velocity, Double Friction.

The dynamical equations were developed for the system, and forward integrated using the Runge-Kutta scheme. The time-step used was 0.003 seconds. The main lesson is the importance of using the correct friction model.

Test Drop

The next step would be to fully develop the simulation into the test drop simulation. Adding a spring and a small lumped mass between the strut and the fixed reference point validated the test drop conditions. This changes the model into a two-degree of freedom system.

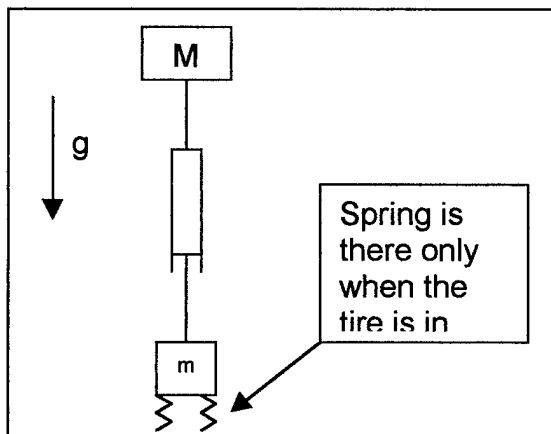


Figure 19. Test Drop Diagram.

- The tire is in contact with the ground
 - The velocity is above the friction cut-off velocity
 - The velocity is below the friction cut-off velocity
- The tire is above the ground
 - The velocity is above the friction cut-off velocity
 - The velocity is below the friction cut-off velocity

Figure 20. Equation Decision Chart.

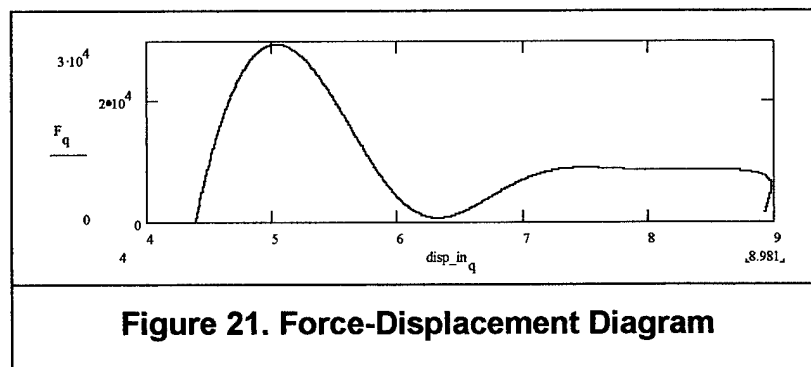
The addition of the tire model creates several complications in both the modeling of the tire itself and of how it interacts with the entire system. The tires behave very linearly, so for simplicity the

spring is modeled as a linear spring. The dynamical equations must also have some conditions on it so that the tire effects are only present when the tire is in contact with the ground. Figure 20 shows that the final equation is dependent on a decision algorithm, making the equation change with the values being integrated.

These decision criteria can be transformed into two simultaneous four part conditional equations. Again, the Runge-Kutta forward integration scheme was used, this time with a time step of 0.0006 seconds. The time-step is smaller than the earlier example because the stability is decreased due to higher frequencies in the system. This simple model does not warrant the use of an unconditionally stable integration scheme, but one could be used effectively in this situation. The conditional equations lend themselves easily to using MathCad's fixed interval Runge-Kutta to evaluate them.

Results

The integration produced the results that follow. They compare well to the general pattern seen in plots from other experiments and models. The main discrepancy comes in the force displacement diagram. It fluctuates from positive to negative force through the compression. Also, because the aircraft bounces, the final compression starts at conditions far different from the initial conditions that started the integration. It is beset to compare the last phase of the compression from when the force becomes positive until the direction reverses. This resembles the normal compression of an oleo-pneumatic strut, with the exception of greater variation in the force load, most likely resulting from the lack of a metering pin model that would regulate the flow rate.



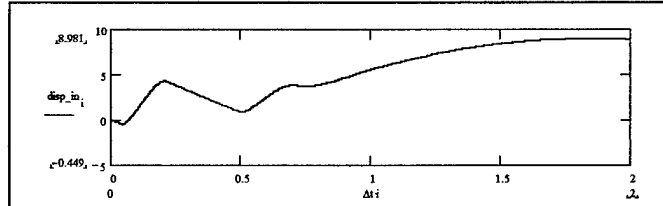


Figure 22. Time-Displacement Diagram for Test Drop.

The displacement shown in the above Figure 22 is the stroke, defined as the displacement from the extended length (positive in the compressive direction). It is possible to see that the model does not quite represent the pre-load correctly, because the displacement becomes negative just after the model has started. This is during the time while the strut is falling but has not reached contact with the ground. Comparing the change in displacement to the ground force pictured in Figure 23 shows that more easily. It also displays the relationship between rate of displacement and the force the ground exerts on the strut.

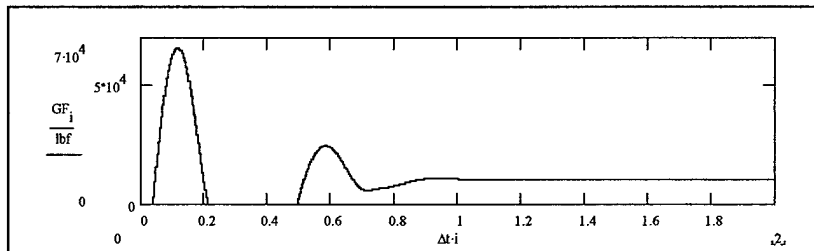


Figure 23. Ground Reaction Force.

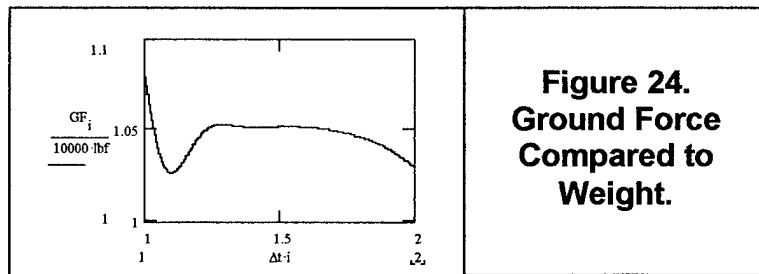
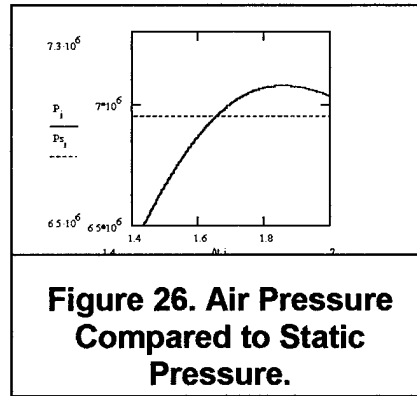
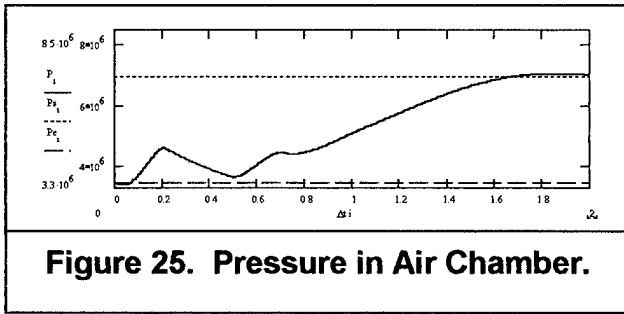


Figure 24. Ground Force Compared to Weight.

Figure 24 shows the ground force in the second half of the model as a multiple of the static load. Although the load is not equal to the weight, it is approaching the weight, showing the validity of the better friction model under quasi-static loading conditions. The same validation can be seen in the air pressure shown in figures below.



The air pressure is a function of the displacement only, if the gas law has an assumed constant exponent. These figures therefore, also show the information concerning the deflection. The air pressure starts at the extended pressure, momentarily dropping below it because of the lack of a stop in the model at the fully extended length. The pressure finishes by quickly approaching the static pressure, slightly overshooting, and oscillating back towards it. This is what is expected of a damped spring mass system.

Conclusions

The Working Model of the landing gear retraction worked well in producing a load deflection graph, which compared well to the expected force time plot. The actuator model was the weak link in the model, because it could only be modeled as either constant velocity or constant force. The model would be more accurate if the assumptions about the component shapes could be refined or if the model was made to represent the three-dimensionality of the real system. Even with these assumptions the model performed very well. The most room for improvement in the modeling would come from inclusion of the actuator model into the numerical model.

The strut model worked very well, but still left room for improvement. The first area would be to obtain a model for the metering pin to be included in the system. It is a very important element used to regulate the force and create greater efficiency. It was easy to see that our model did not have a metering pin because of the major fluctuation in the force displacement diagram.

Another area of improvement is that of the gas law exponent. The system acts much more isotropically at low velocity when the mixing of oil and gas is small, and more polytropically when the compression rate is high and the oil spatters, foams, and otherwise mixes with the gas. A variable exponent may be able to give better results.

The friction model is also of need for help. The cut off velocity of one foot per second was very arbitrary, and selected mainly for the continuity it would preserve in the equation. A better analysis of the friction model should be done and incorporated into the model as a whole.

Without a doubt, the modeling worked well for being such a first elementary model of these systems. Refinement can always be done in an effort to get more exact, but this does model the general behavior quite well.

References

1. REDDY J.P., NAGARAJ V.T. and RAMAMURTI V., "Analysis of articulated landing gear behavior", *Proceedings of the Sixth World Congress on Theory of Mechanics and Mechanisms*, 1983
2. WALLS J.H., Investigating of the air compression process during drop test of an oleo-pneumatic landing gear, NACA TN 2477, Sept. 1951
3. BAZZOCCHI E., Method de calcul des amortisseurs oleopneumatiques et comparaison avec les resultats d'essais obtenue, *Technique et science (Aeronautique)*, 3 rd March, 1956
4. WAHI M.K., Oleopneumatic shock strut dynamic analysis and its real time simulation, *AIAA Journal of Aircraft*, Vol. 13. No. 4, April 1976
5. CARDONA, A. *Modeling of a Hydraulic Actuator in a Finite Element Mechanism Analysis Program*, PhD Thesis, "An Integrated Approach to Mechanism Analysis", University of Liege, 1989
6. CURREY N.S., *Aircraft Landing Gear Design: Principles and Practices*, AIAA Education Series, 1988
7. D'AZZO J.J., HOUPIS, C.H. *Linear System Analysis and Design: Conventional and Modern*, McGraw Hill, 1975